Guidance and control of a reconfigurable unmanned underwater vehicle

M. Caccia*, G. Veruggio

Consiglio Nazionale delle Ricerche, Istituto per l'Automazione Navale, Via De Marini, 6, 16149 Genova, Italy

Abstract

The problem of designing, implementing and testing a general-purpose guidance and control system for unmanned underwater vehicles for scientific applications is addressed in this paper. A three-level hierarchical architecture is proposed in order to uncouple the execution of user-defined motion-task functions with respect to the operating environment (guidance), from linear and angular speed control and mapping of the required control actions onto the actuation system. The introduction of PI-type task functions enables a conventional Lyapunov-based guidance system to counteract the effects both of unmodelled, i.e. unmeasured kinematic interactions between the vehicle and the environment, and of bias in velocity measurements. The vehicle dynamics are managed by conventional gain scheduling regulators performing velocity control, while an advanced actuator model, which considers propeller–hull interactions, improves the precision of the thrust to propeller rate mapping. Preliminary tests, carried out in a high-diving pool with an over-actuated prototype ROV, proved the system's functionality and showed high performances in terms of its precision in accomplishing near bottom slow motion tasks, e.g. altitude and hovering control and trajectory tracking, even when the mapping of the required control actions onto the actuation system is reconfigured to face any type of thruster fault. © 2000 Elsevier Science Ltd. All rights reserved.

Keywords: Control; Guidance systems; Underwater vehicles

1. Introduction

Scientific investigations in physical, chemical, geological and biological processes in the marine environment often require the use of unmanned underwater vehicles (UUVs) to perform exploration, survey, monitoring and data collection tasks that reduce ship costs and human risks. This is true in the case of autonomous underwater vehicles (AUVs), such as the Autonomous Benthic Explorer (Yoerger, Bradley & Walden, 1993; Singh, Yoerger, Bachmayer, Bradley & Stewart, 1995), Odyssey II (Bellingham, Goudey, Consi, Bales, Atwood, Leonard & Chryssostomidis, 1994) and Ocean Explorer (Smith, Heeb, Frolund & Pantelakis, 1995), employed in missions to survey and gather oceanographic and geological data, and of remotely operated vehicles (ROVs),

such as Victor (Nokin, 1996), Tiburon (Newman & Stokes, 1994) and Romeo (Caccia, Bono, Bruzzone & Veruggio, 1999b), employed to collect pelagic and benthic images, data and samples. In particular, near bottom applications, such as the quantitative and qualitative observation of benthic life and the collection of samples to study the water–sediment interface (Smith, Terribile & Finottello, 1998), require high levels of motion control in terms of agility and precision (of the order of a few centimetres), and minimisation of environmental perturbations caused by the actuation system. As observed in Sayers, Yoerger and Paul (1996) and Veruggio, Bono, Bruzzone, Caccia and Virgili (1998), the unpredictability of the subsea environment and the limitations of the state-of-the-art machine-intelligence techniques makes real-world operations, which require a close robot–environment interaction, reliable only when human intervention is possible. On the basis of these considerations, advanced scientific ROVs are currently designed as teleoperated systems, which can automatically execute a set of motion functions (position and speed control) and enable the human operator to interact with each level of

* Corresponding author. Tel.: + 39-010-647561; fax: + 39-10-6475600.
E-mail addresses: max@ian.ge.cnr.it (M. Caccia), gian@ian.ge.cnr.it (G. Veruggio)

the control architecture (Sheridan, 1989). This is the case, for instance, in typical scientific seabed explorations, which are performed by ROVs combining automatic position-level heading and altitude control with speed-level surge and sway control. During sediment sampling the operator can directly control the vertical thrust of the vehicle too. In addition, the adoption of a redundant, fully controllable and fault tolerant actuator configuration enhances the vehicle's motion control performances and reliability, increasing its capability in accomplishing a mission even in the presence of unexpected problems, thus optimising the exploitation of expensive and complex logistics for oceanic operations.

In the following sections the problem of designing, implementing and testing a modular and portable guidance and control architecture for ROVs for scientific applications is addressed. In addition to the application-related performance and operational requirements mentioned earlier, the proposed control system basically has to manage the nonlinear, coupled and unpredictable hydrodynamics typical of unstreamlined open-framed ROVs. Conventional approaches to overcome the unpredictable behaviour of these vehicles rely on robust trajectory-control techniques using sliding modes (Yoerger & Slotine, 1985). In Healey and Lienard (1993), a set of sliding mode controllers, characterized by sliding surfaces based on variable state errors rather than output errors as in Yoerger and Slotine (1985), has been applied to design a UUV control system consisting of three basic autopilots for steering, diving and speed control. Sliding mode control has proved its capability in handling an uncertainty of the order of 50% in the estimation of the vehicle's hydrodynamic parameters in the case of the heading and depth control of the autonomous underwater shuttle SIRENE (Silvestre, Aguiar, Oliveira & Pascoal, 1998). On the other hand, robustness has been achieved by means of adaptive control schemes, including hybrid adaptive and sliding mode techniques, as discussed in Fossen and Sagatun (1991) and Fossen and Fjellstad (1995). In all these cases, the guidance system consisted of a conventional line-of-sight (LOS) algorithm generating the reference heading and, sometimes, surge velocity. A LOS-type reference heading, steering the vehicle towards the point to be reached, has also been obtained, using a Lyapunov-based guidance algorithm to approach a target area, regardless of vehicle's orientation, as shown by Caccia, Casalino, Cristi and Veruggio (1998), where a guidance and control scheme based on an outer control loop generating reference values for inner speed controllers to execute user-defined task functions has been integrated with a conventional UUV autopilot performing autoheading, autodepth and autospeed. This approach, which does not require any (re)planning, proved its feasibility in controlling the vehicle's motion in the presence of a high uncertainty in position estimates, typical of underwater robotics, and, because of its Lyapunov-based (i.e. potential field) nature, seems to be suitable for accomplishing reactive guidance tasks in unknown environments. On the basis of this experience a set of controllers of the vehicle's linear and angular velocities has been introduced to exploit the potentialities of a Lyapunov-based guidance system design, which naturally generates reference velocities for the control level (Aicardi, Caiti, Cannata & Casalino, 1995). The result has been a three-level hierarchical architecture able to uncouple the management of the actuation system, the vehicle's dynamics and its kinematics. The guidance level executes the user-defined task functions dealing with the kinematic interactions between the robot and the operating environment, i.e. position control of the vehicle with respect to an environment-fixed reference frame, e.g. depth control, or detected environmental features, e.g. altitude control. The control level is task independent and tracks the required velocities handling the vehicle's dynamics by means of a set of model-based uncoupled controllers. The required control actions, force and torque, generated by the speed regulators are mapped onto the vehicle actuator thrusts by the actuation system module, which takes account of the vehicle's thruster configuration. It is worth noting that conventional ROV autopilots can be implemented in this framework by a suitable combination of guidance position task functions and velocity controls. The mapping of the control force and torque onto the vehicle thrusters is performed by applying the classical Moore–Penrose pseudo-inverse method (Fossen, 1994) to a lumped parameter actuator model including propeller–hull interactions, which are not negligible in the case of open-frame ROVs (Caccia et al., 1999b). A set of gain scheduling proportional-integral (PI) velocity controllers constitutes the control level, where unmodelled dynamics, errors in the estimate of the hydrodynamic parameters and external disturbances are compensated by the integrator. As discussed before, the guidance level consists of a set of Lyapunov-based controllers executing motion task functions: a relevant enhancement in precision performances is allowed by the introduction of PI-type task functions, which enable the system to handle unmodelled, i.e. not measured or estimated, kinematics interactions between the robot and the operating environment. The resulting control system has been tested on the prototype ROV Romeo, developed by the CNR-IAN Robotics Department for marine science applications and robotics research in the field of intelligent vehicles. During the tests, attention has been focused on verifying the system's capability in executing accurate hovering and altitude control in proximity of the bottom as required by scientific users (Smith et al., 1998). The paper is organized as follows. Section 2 reports basic modelling and notation for the dynamics and kinematics of underwater vehicles. The guidance and control architecture is presented in Section 3, where algorithmic details are given and a set of

basic task functions is introduced. A brief note on the combined estimate of the vehicle depth and altitude in hovering conditions is also reported. Section 4 deals with the actuator management system, discussing the optimal mapping of the control action in the case of a redundant actuation system, and an advanced propeller model able to simply take account of the propeller–hull interactions. In Section 5, the ROV Romeo is presented, focusing attention on its mechanical design and thruster configuration, and pool and simulative test results are reported. In-water trials showed the satisfying performances of the control system in linear speed control and in executing hovering and altitude task functions, even while working with different thruster configurations. The performance improvements obtained by using PI-type guidance laws are also pointed out by a simulative example of a bottom following application without any estimate of the sea floor profile.

2. Modelling

Since most open-frame vehicles are intrinsically stable in pitch and roll, a simplified model for UUV dynamics has been considered, neglecting pitch and roll motions. Anyway, a complete treatment of the modelling of underwater vehicles can be found in Newman (1977), Yuh (1990) and Fossen (1994). Usually, the vehicle's position and orientation $[x\ y\ z\ \psi]$ are referred to an inertial environmentally fixed reference frame $\langle e \rangle$, while the linear and angular velocities are defined in a vehicle-fixed reference frame $\langle v \rangle$, which, neglecting pitch and roll, is rotated about the angle ψ on the horizontal plane with respect to the frame $\langle e \rangle$ (see Fig. 1).

The vehicle hydrodynamics is modelled with respect to the frame $\langle v \rangle$ as follows:

$$
\begin{aligned}
m_u \dot{u} &= m_v vr - k_u u - k_{u|u|} u|u| + F_u, \\
m_v \dot{v} &= -m_u ur - k_v v - k_{v|v|} v|v| + F_v, \\
m_w \dot{w} &= -k_w w - k_{w|w|} w|w| + F_w + W, \\
I_r \dot{r} &= -(m_v - m_u)uv - k_r r - k_{r|r|} r|r| + T_r,
\end{aligned}
\tag{1}
$$

where u, v, w and r are the vehicle linear and rotational velocities with respect to the water (surge, sway, heave and yaw, respectively), m_u, m_v, m_w and I_r are the vehicle masses and moment of inertia (including added mass and inertia), and hydrodynamic damping is modelled as a linear and a quadratic term. F_u, F_v and F_w are the forces applied by the thrusters along the surge, sway and heave directions, T_r is the torque in the yaw motion and W is the resultant of the vehicle weight and buoyancy. Assuming that the vehicle is moving in a constant horizontal current field, the absolute horizontal velocities of the
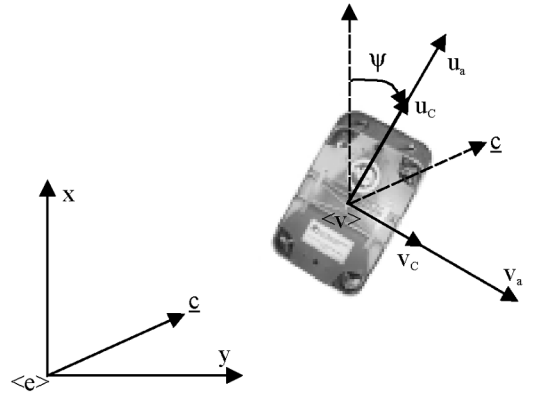

Fig. 1. Environmental- and vehicle-fixed reference frames (the axes z and w are directed inwards).

vehicle with respect to the frame $\langle v \rangle$ are

$$
\begin{aligned}
u_a &= u + u_C, \\
v_a &= v + v_C
\end{aligned}
\tag{2}
$$

with

$$
\begin{aligned}
\dot{u}_C &= v_C r, \\
\dot{v}_C &= -u_C r,
\end{aligned}
\tag{3}
$$

where $[u_C\ v_C]^{\mathrm{T}}$ represents the current field in the vehicle-fixed reference frame. At last, the vehicle kinematics is modelled by the state equations

$$
\begin{aligned}
\dot{x} &= u_a \cos \psi - v_a \sin \psi, \\
\dot{y} &= u_a \sin \psi + v_a \cos \psi, \\
\dot{z} &= w, \\
\dot{\psi} &= r.
\end{aligned}
\tag{4}
$$

3. Guidance and control architecture

The proposed guidance and control system is based on a two-layered hierarchical architecture for closed-loop control of the class presented in Aicardi et al. (1995). As shown in Fig. 2, the inner control loop is task independent and implements a velocity servo loop that is based on the exact, or even approximated knowledge of the vehicle dynamics. On the other hand, the outer guidance loop deals with the kinematics of the vehicle–environment interactions and generates the reference velocities for the control in order to accomplish the user-defined task functions (Samson, Le Borgne & Espiau, 1991). In particular, a Lyapunov-based design enables the guidance module to eliminate operational errors without requiring any on-line or off-line trajectory (re)planning.

Referring to Fig. 2, the operational variables χ, which are functions of the vehicle position/orientation and its
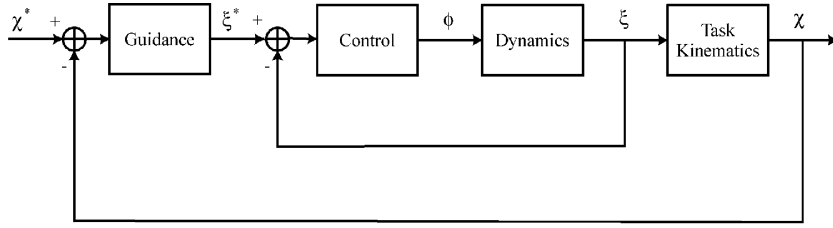
Fig. 2. Guidance and control architecture.

interactions with the operating environment, are represented in an environmentally fixed reference frame, while the controlled velocities ξ are defined with respect to a vehicle-fixed reference frame. The control force and torque are indicated with ϕ.

3.1. Guidance

The synthesis of the guidance controller is based on the definition of a positive-definite function V of a task function $\mathbf{e}$, $V(\mathbf{e}) = \frac{1}{2}\mathbf{e}^T\mathbf{e}$. If the reference velocities are chosen so that $\dot{\mathbf{e}} = -\lambda\mathbf{e}$, then $\dot{V}$ is a negative definite and V is a Lyapunov function with a stable equilibrium point $\mathbf{e} = \mathbf{0}$.

As discussed in Aicardi et al. (1995), the task function $\mathbf{e}$ can represent the position/orientation errors having the form $\mathbf{e} = \chi - \chi^*$, a task function of P-type. In this case, assuming the reference operational constant are variables, if a linear invertible mapping $\dot{\chi} = L\xi$ exists, a suitable choice of the desired velocities is

$$\xi^* = -\lambda L^{-1}(\chi - \chi^*). \tag{5}$$

In underwater robotic applications the presence of a bias in the speed measurements and estimates is quite common (e.g. Doppler velocimeter bias or model-based nonlinear biased estimators such as an extended Kalman filter). This fact determines a non-zero mean error in the velocity tracking, which acts as a disturbance in the guidance loop and could be counteracted by a high gain λ, which can cause instability or limit-cycling problems due to system non-linearities and bandwidth limitations. To avoid this problem an integrator can be included in the guidance regulator, defining a task function of PI-type $\mathbf{e} = (\chi - \chi^*) + \mu\int_0^t(\chi - \chi^*)\,d\tau$. In this case, the desired velocities can be chosen as

$$\xi^* = -\lambda_P L^{-1}(\chi - \chi^*) - \lambda_{IL}^{-1}\int_0^t(\chi - \chi^*)\,d\tau,$$

$$\text{with } \lambda_P = \lambda + \mu, \lambda_I = \lambda\mu, \lambda > 0, \mu > 0. \tag{6}$$

It is worth noting that the integral action can also compensate for the speed disturbances induced by unmodelled kinematics interactions between the robot and the operating environment.

If the Controller is able to guarantee a norm bounded velocity error, these guidance laws guarantee to annul the error in tracking the reference operational variables, provided that the gain is sufficiently high.

The wind-up effects can be avoided by saturating the integral and switching on the integrator only when the task error $\|\mathbf{e}\|$ is minor than a suitable threshold, otherwise a P-type guidance law is active. Steady-state properties of the proportional regulator guarantee that the system reaches the switching condition. In order to avoid chattering between PI- and P-guidance task functions due to the noise in the position estimate, a hysteresis mechanism has to be implemented.

In the following, a set of task functions related to the implementation of a conventional Autopilot and the execution of hovering and altitude control are presented. As discussed below, the execution of these motion tasks involves different degrees of interaction with the operating environment and capabilities in motion estimation.

3.1.1. Conventional autopilot

Conventional ROV autopilots usually perform automatic control of the vehicle's heading and depth (Perry Tritech Ltd., 1996). In these cases the couple (χ, ξ) coincides with (ψ, r) and (z, w) respectively, and, assuming, for instance, a P-type task function, the reference yaw rate and heave are computed as $r^* = -\lambda_\Psi(\psi - \psi^*)$ and $w^* = -\lambda_z(z - z^*)$.

3.1.2. Hovering

When the task is hovering over a target area, i.e. remaining in a fixed horizontal position $\chi^* = [x^* \; y^*]^T$, the operational variables $\chi = [x \; y]^T$ and the vehicle surge and sway velocities, $\xi = [u_a \; v_a]^T$, are considered. According to the choice of a P- or PI-type task function, the desired velocities ξ^* are, respectively, computed from Eqs. (5) or (6), where the linear mapping L assumes the form (see (4))

$$L = \begin{bmatrix} \cos\psi & -\sin\psi \\ \sin\psi & \cos\psi \end{bmatrix}.$$

In particular, when a PI-type task function is considered, the following reference speeds are computed:

$$u_a^* = -\lambda_P[(x - x^*)\cos\psi + (y - y^*)\sin\psi]$$

$$-\lambda_I\int_0^t[(x - x^*)\cos\psi + (y - y^*)\sin\psi]\,d\tau,$$

$$v_a^* = -\lambda_P[-(x-x^*)\sin\psi + (y-y^*)\cos\psi]$$

$$-\lambda_I \int_0^t [-(x-x^*)\sin\psi + (y-y^*)\cos\psi]\,d\tau. \quad (7)$$

3.1.3. Auto-altitude

In accomplishing the task of *bottom-following*, i.e. "maintaining a fixed altitude above an arbitrary surface whose characteristics may or may not be known" (Bennett, Leonard & Bellingham, 1995), the operational variable, i.e the altitude respect to the seabed, represents an interaction between the robot and the operating environment.

In the general situation depicted in Fig. 3, the vehicle is assumed to execute linear traverses in the surge direction, i.e. $u_a \neq 0$ and $v_a = 0$. Indicating the local slope of the seabed in the direction of the motion with α, and the vehicle altitude with h, its first time derivative is

$$\dot{h} = -u_a \tan\alpha - w, \quad \alpha \in \left(-\frac{\pi}{2}, \frac{\pi}{2}\right).$$

A suitable guidance algorithm for this general situation is presented in Caccia, Bruzzone and Veruggio (1999a). When the vehicle is asked to hover over an area of special interest, i.e. the horizontal speed is assumed to be zero, applying a P-type guidance algorithm, the *altitude control* law reduces to a simple proportional *vertical position controller*, $w^* = \lambda(h - h^*)$, $\lambda > 0$, which does not require any information about the terrain slope. The same simplified kinematics model $\dot{h} = -w$, neglecting the effects of the vehicle horizontal motion and seabed slope, can be used to synthesize a PI-type bottom-following controller, whose integral action compensates the unmodelled velocity $-u_a \tan\alpha$, $\alpha \in (-\pi/2, \pi/2)$.

3.2. Control

A set of uncoupled speed controllers based on the vehicle's model described by Eq. (1) have been designed. Neglecting any interaction between the motion of the vehicle along different axes, the dynamics with respect to
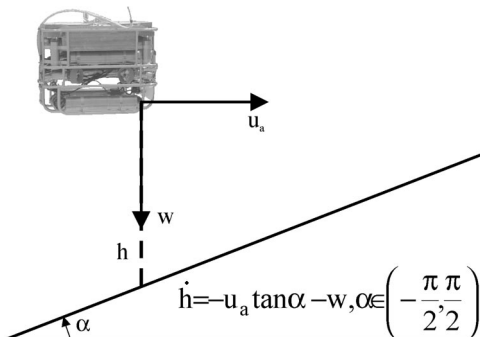

Fig. 3. Bottom-following operational variables.

the water along/around each axis is of the form:

$$\dot{\xi} = -\frac{k_\xi}{m_\xi}\xi - \frac{k_{\xi|\xi|}}{m_\xi}\xi|\xi| + \frac{1}{m_\xi}\phi, \quad (8)$$

where ξ is the linear/angular speed and ϕ is the external force/torque applied to the vehicle.

According to the gain-scheduling design technique presented in Khalil (1996), at each constant operating point, the controller provides a feed-forward constant control value $\bar{\phi}$ yielding zero error and an additional feed-back control action ϕ_δ, which assigns a desired characteristic equation to the closed-loop linearised system. In this way, the controller assumes the form $\phi = \bar{\phi} + \phi_\delta$.

For every value of the reference speed ξ^* in the operating range, a feed-forward control value $\bar{\phi}(\xi^*) = k_\xi\xi^* + k_{\xi|\xi|}\xi^*|\xi^*|$ is applied, and the nonlinear state-equation (8) is linearised about the desired operating point $(\xi, \phi) = (\xi^*, \bar{\phi})$, obtaining the family of parameterized linear models

$$\dot{\xi}_\delta = -a(\xi^*)\xi_\delta + b\phi_\delta, \quad (9)$$

where

$$a(\xi^*) = \frac{k_\xi + 2k_{\xi|\xi|}|\xi^*|}{m_\xi} \quad \text{and} \quad b = \frac{1}{m_\xi}.$$

In order to force the tracking error to be zero at equilibrium in the presence of parameter perturbations and disturbances (e.g., errors in the estimation of the drag coefficients or the resultant W of the vehicle's weight and buoyancy), a PI controller for the linearised system is designed. In the same way, this controller structure compensates for any horizontal current disturbance, which can be modelled as the effect of a constant force disturbance when the vehicle operates with fixed orientation, e.g. executing traverses or hovering.

In order to obtain a desired characteristic equation for the closed-loop linearised system of the form

$$s^2 + 2\sigma s + \sigma^2 + \omega_n^2 = 0, \quad (10)$$

the gains k_P and k_I of the PI-controller $\phi_\delta = k_P e + k_I\gamma$, $\dot{\gamma} = e = \xi^* - \xi = \xi_\delta$ are scheduled as functions of ξ^* according to the formulae $k_P = m_\xi(2\sigma - a) = 2m_\xi\sigma - k_\xi - 2k_{\xi|\xi|}|\xi^*|$ and $k_I = m_\xi(\sigma^2 + \omega_n^2)$.

3.3. Motion estimation

The motion of a UUV during "at sea" operations is measured by a set of sensors with different performances and possibilities of use. Heading and yaw rate measurements are provided by compass and gyro, while the horizontal position and speed can be measured by acoustic positioning systems (e.g. Long Base Line and Super Short Base Line positioning systems) and Doppler

velocimeters. Anyway, LBL and SSBL data are not accurate enough to satisfy requirements for fine motion control (Ageev, Kasatkin & Scherbatyuk, 1995) and Doppler devices do not work in the proximity of the seabed, i.e. when the vehicle's altitude is less than 1 m. Therefore, during scientific benthic operations the vehicle's horizontal position and speed are expected to be evaluated by vision-based systems (Maddalena, Prendin & Zampato, 1994; Negahdaripour, Xu & Khamene, 1998). On the other hand, the vehicle's depth and altitude are usually measured by pressure-sensors and echo-sounders, while no direct measure of the vehicle's vertical speed is provided.

Kinematic estimators such as linear Kalman filter or complementary filters (Fryxell, Oliveira, Pascoal, Silvestre & Kaminer, 1996) provide a good estimate of the vehicle's motion when linear/angular position and velocity measurements are supplied, as in the case of heading and yaw rate estimators and of multi-rate complementary filters for horizontal motion estimation based on compass, LBL and Doppler velocimeter measurements (Oliveira and Pascoal, 1998). When no speed measurements are available, model-based estimators are generally used. In particular, extended Kalman filters with a time-varying augmented measurement model and a common dynamic representation for the state has proved to be a useful approach in handling multi-rate measurement systems (Krieg & Gray, 1996). In the following an application of eKf for the combined estimate of the vehicle depth and altitude for near-bottom hovering operations is presented. The problem of eliminating the tracking errors induced by the use of biased estimators has been addressed in Section 3.1 introducing the PI-type task-functions for the vehicle guidance.

3.3.1. Vertical motion estimation

During benthic scientific missions the vehicle is required to hover over the seabed at an altitude of a few centimeters. To this aim, a very accurate estimate of the vehicle's altitude, depth and heave is needed. When the seabed depth can be assumed to be constant, the estimate of the vehicle's vertical motion is improved by the processing of the acoustic measurements of its altitude, which are usually taken at a low sampling rate, but more precisely than that of the pressure-meter data. To this aim, the state of the dynamic system describing the vehicle's vertical motion, i.e. depth, heave and weight-buoyancy force $[z\ w\ W]^{\mathrm{T}}$, is augmented introducing the seabed depth in the working area, which models the operating environment. The following dynamic system is obtained:

$$\dot{z} = w$$
$$\dot{w} = -\frac{k_w}{m_w}w - \frac{k_{w|w|}}{m_w}w|w| + \frac{1}{m_w}F_w + \frac{1}{m_w}W,$$
$$\dot{W} = 0,$$
$$\dot{s} = 0,$$
(11)

where the seabed depth s is assumed to be constant because the vehicle is supposed to hover over the operating area. Defining the altitude as $h = s - z$, the measurement equations are $\begin{cases} z_m = z + v_z \\ \rho = s - z + v_\rho \end{cases}$, where z_m and ρ are the depth-meter and echo-sounder altimeter data, respectively, supposedly affected by zero mean Gaussian noises. As mentioned before, extended Kalman filter techniques have proved their feasibility in estimating the state $\underline{x} = [z\ w\ W\ s]^{\mathrm{T}}$, by handling the different sampling rates of the depth-meter and altimeter.

4. Actuator management system

The guidance and control system described in the previous section computes the force and torque to be applied to the vehicle in order to perform user-defined motion task functions. The following addresses the problem of mapping the required control actions on the propeller revolution rates for an over-actuated open-frame ROV. A two-layered scheme, which separates the mapping of the required force–torque on the actuator thrusts from the computation of the suitable propeller revolution rates, is proposed. The propeller velocity control is usually performed by hardware servo-amplifiers for DC motors and its time constant is negligible with respect to the system's dynamics (Yuh, 1994).

4.1. Control force–torque to actuator thrusts mapping

The resultant force–torque exerted by the vehicle actuators can be computed as $\phi = B\tau$, where $B \in \Re^{m,n}$ is the control matrix, and τ, the vector of the actuator thrusts. In the case of over-actuated vehicles, B is non-square with $m < n$ and $\mathrm{rank}(B) = m$, that is, there are more control inputs than controllable DOFs, and it is possible to find "optimal" distributions of the control actions, satisfying some physical constraints or minimizing a particular cost function.

A general purpose choice involves minimising the quadratic energy cost function $J = \frac{1}{2}\tau^{\mathrm{T}}P\tau$, which, in cases where all inputs are equally weighed, has the solution $B^{\#} = B^{\mathrm{T}}(BB^{\mathrm{T}})^{-1}$, known as the Moore–Penrose pseudo-inverse (Fossen, 1994). For the square case, as when faulted actuators are disabled, $B^{\#}$ is simply equal to B^{-1}, and the unique solution is computed.

4.2. Thrust to propeller rate mapping

Once the desired actuator thrust has been determined, the reference propeller revolution rate for the servo-amplifiers can be computed. The nominal propeller I/O relationship has the bilinear form $\tau = a_n n|n| - b_n v_a n$, where τ and n are the propeller thrust and revolution

rate, v_a is the advance speed, i.e. the speed of the water inside the blades of the propeller, and a_n, b_n are positive constants. In the case of open-frame ROVs operating at low speed, the bilinear model can be approximated by an affine model of the propeller working at bollard conditions, i.e. the advance speed is zero, $\tau = a_n n|n|$. The parameter a_n, which usually has different values for positive and negative propeller rotations, can be identified for an isolated thruster by means of thrust-tunnel tests. Anyway, in the case of open-frame ROVs the propeller–hull interactions cannot be neglected. A suitable model for the reduction in the thruster efficiency when the propeller boosts the water against the vehicle hull is proposed in Caccia et al. (1999b). Assuming the propeller works in free water when the revolution rate n is positive, a thruster efficiency coefficient η is introduced so that

$$\eta = 1, \quad \text{if } n \geqslant 0,$$
$$\eta = \eta^*, \quad 0 < \eta^* \leqslant 1, \quad \text{otherwise},$$

where the parameter η^* can be identified by suitable in-water tests of the vehicle (Alessandri, Bono, Caccia, Indiveri & Veruggio, 1998; Caccia et al., 1999b). In this way, the propeller I/O relationship for open-frame ROVs assumes the form $\tau = \eta a_n n|n|, 0 < \eta \leqslant 1$, and, since $\text{sign}(n) = \text{sign}(\tau)$, the reference revolution rate is computed as $n = \sqrt{|\tau|/\eta a_n} \, \text{sign}(\tau)$.

5. Applications

The guidance, control and actuator management systems for unmanned underwater vehicles described in the previous sections have been implemented and tested on Romeo, an over-actuated open-frame ROV developed by the CNR-IAN for robotics research and scientific applications. In the following, a brief description of the vehicle's mechanical design is given, focusing on its thruster configuration. More detailed information about Romeo computer and software design can be found in Caccia et al. (1999b). Experimental results demonstrating the functionality of the proposed control system are reported and discussed.

5.1. Romeo's mechanical design and thruster configuration

Romeo's mechanical design follows the structure of the last generation of scientific ROVs, such as Tiburon (Kirkwood, 1998) and Victor (Nokin, 1998). The vehicle, which is about 1 m in height, 0.9 m in width and 1.3 m in length, weighs about 450 kg in air and is intrinsically stable in pitch and roll, is divided into three sections. The bottom section of the vehicle carries an interchangeable toolsled for scientific devices, which in the standard version is equipped with two cylindrical canisters for batte-

ries and payload electronics. The middle section, the core vehicle, is made up of a basic frame carrying one 100×32 cm (ld) cylindrical canister for the control system, plant management and communications electronics, two 80×15 cm (ld) cylinders for batteries and battery chargers, one 60×15 cm (ld) cylinder for compass, gyro, and inclinometers, four thrusters for propulsion in the horizontal plane, four for the vertical propulsion, and the basic sensor package (CTD, pilot and scientist TV cameras, etc.). The top section, carried by the basic frame, is made up of foam for buoyancy. The thrusters, canisters, and instruments are allocated so that the overall structure of the vehicle is symmetric with respect to both the xz and yz planes. As shown in Fig. 4, the thrusters are arranged two by two in the corners, with the horizontal ones parallel to the diagonals of the xy section. This thruster configuration enables full control of the vehicle's motion even in cases of faults in one horizontal or vertical actuator, making space available for vision devices in front of the vehicle and for electronics equipment in the middle. In addition, the allocation of the vertical propellers on the top of the vehicle reduces their pull-up efficiency because of propeller–hull interactions, but minimizes the interactions between the boosted water and the sediments during benthic operations, satisfying a basic scientific requirement.

The desired force and torque are mapped onto the Romeo thrusters according to the algorithm discussed in Section 4.1, uncoupling the horizontal control of surge, sway and yaw, from the vertical control of roll, pitch and heave. Calling the module of the angle between the horizontal thrusters and the vehicle's longitudinal axis α, b, c and d the thruster arms with respect to the vehicle's centre of mass for yaw, roll and pitch motion, respectively, two normalized horizontal and vertical force and torque vectors $\phi_H = [F_u/\cos \alpha \quad F_v/\sin \alpha \quad T_r/b]^T$ and $\phi_V = [T_p/c \quad T_q/d \quad F_w]^T$, and control matrixes

$$B_H = \begin{bmatrix} 1 & 1 & -1 & -1 \\ 1 & -1 & 1 & -1 \\ 1 & -1 & -1 & 1 \end{bmatrix}$$

and

$$B_V = \begin{bmatrix} -1 & 1 & -1 & 1 \\ -1 & -1 & 1 & 1 \\ 1 & 1 & 1 & 1 \end{bmatrix},$$

are defined such that $\phi_H = B_H \tau_H$ and $\phi_V = B_V \tau_V$, where $\tau_H = [\tau_{HFL} \ \tau_{HFR} \ \tau_{HRL} \ \tau_{HRR}]^T$ and $\tau_V = [\tau_{VFL} \ \tau_{VFR} \ \tau_{VRL} \ \tau_{VRR}]^T$ are the horizontal and vertical vectors of the actuator thrusts. It is worth noting that as a consequence of the symmetries in thruster configuration, if τ_H^* is a solution of the horizontal mapping problem then $\tau_H^* + \Delta \tau_H$ is still an acceptable solution. In this way, it is possible to
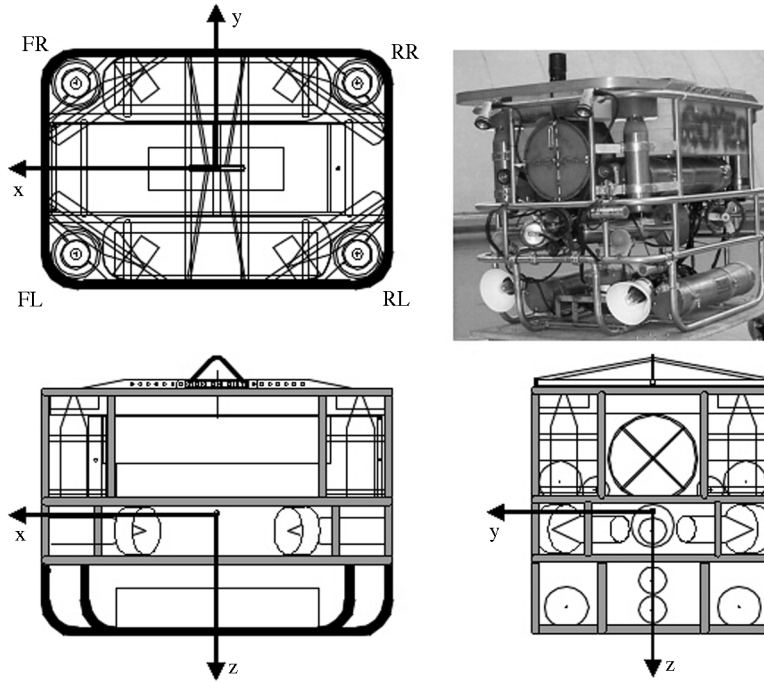
Fig. 4. Romeo mechanical design.

choose an optimum propeller working point, in the presence of actuators that are strongly nonlinear, e.g. characterized by a round-zero dead-zone. In addition, when no roll and pitch torque is required, the vertical mapping solutions are characterized by $\tau_{VFL} = \tau_{VRR}$ and $\tau_{VFR} = \tau_{VRL}$, and only a couple of diagonally opposite vertical thrusters are sufficient to control the vehicle's vertical motion, with a corresponding reduction in the maximum lift capability and downwards thrust.

5.2. Experimental setup and results

A set of experiments to demonstrate the functionality of the presented UUV Control System in high precision hovering and altitude control has been carried out in a high-diving pool with Romeo. During the experiments the auto-heading task-function maintained the vehicle parallel to the pool walls, enabling a couple of echo-sounders Tritech PA200-20 to measure the vehicle's horizontal position tracking two perpendicular pool walls (see Fig. 5). In this way, assuming $\psi \cong 0$ and $r \cong 0$, Romeo's horizontal position and speed have been estimated via extended Kalman filter on the basis of the simplified model

$$\dot{x} = u,$$
$$\dot{y} = v,$$
$$m_u \dot{u} = -k_u u - k_{u|u|} u|u| + F_u,$$
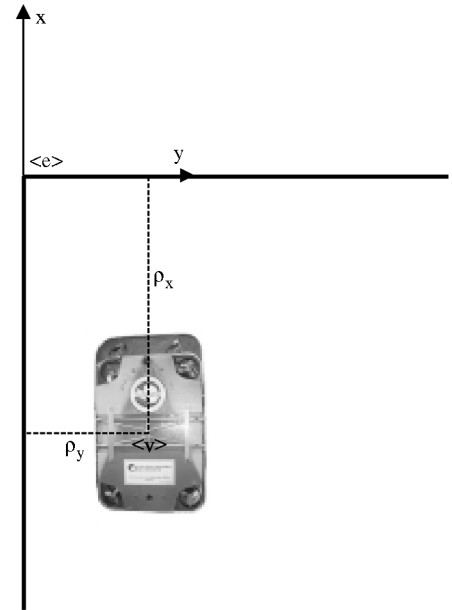$$m_v \dot{v} = -k_v v - k_{v|v|} v|v| + F_v,$$

(12)

Fig. 5. Notation for Romeo pool tests.

where any current is neglected and the measurement equations are $\begin{cases} \rho_x = -x + v_x \\ \rho_y = y + v_y \end{cases}$. The linear and quadratic drag coefficients have been identified by suitable steady-state experiments (Caccia et al., 1998), while the added mass of an *equivalent ellipsoid* has been considered. The sampling rate of the echo-sounders was 3.33 Hz, and

prediction steps were performed by the filter when no new data were available, in order to simulate a generic vision-based motion estimator with bias and noise in the position and speed estimates.

Heading and yaw rate measurements were supplied by a KVH-DG100 compass and low-cost gyro unit (Everett, 1995), and processed by a conventional linear Kalman filter. These devices, as well as the depth-meter, have a sampling rate of 10 Hz. In the conventional operating modes, the vehicle's depth has been estimated by an extended Kalman filter based on the first three equations of (11). Since the goal of the trials was to demonstrate the possibility of operating in the proximity of the bottom, i.e. altitude less than 1 m, a high-frequency pencil beam profiling sonar, Tritech ST-1000 at 1.25 MHz with a sampling rate of 3.33 Hz, has been used as altimeter in order to obtain high precision measurements. Since its minimum operating range is about 35 cm, the sonar was mounted at 50 cm from the bottom of the vehicle. In addition, a 200 KHz Doppler velocimeter RDI-DVL Workhorse Navigator measured the vehicle's speed with a sampling rate of 1 Hz. This device cannot work when the vehicle's altitude is less than 0.8 m.

5.2.1. Speed control

At first, the gain scheduling velocity controllers were tested, proving the capability of the system to be tuned according to different velocity sampling rates. Two typi-cal operational conditions have been considered. In the former, the horizontal speed was measured by the Doppler velocimeter, in the latter the vehicle velocities were estimated on the basis of acoustic-based displacement measurements.

As discussed in Åström and Wittenmark (1989), the natural frequency, $\omega_0 = \sqrt{\sigma^2 + \omega_n^2}$, of the dominating poles of the closed-loop linearised second-order system, see Eq. (10), has been chosen so that $\omega_0 \Delta t \approx 0.1 - 0.5$, where Δt is the sampling rate, and the ratio ω_n/σ has been fixed to 0.1. In particular, the velocities measured by the Doppler velocimeter at 1 Hz were used as direct feed-back for a controller characterized by $\sigma = 0.2$ and $\omega_n = 0.02$, while, when the vehicle's horizontal speed was estimated on the basis of 3.33 Hz sampled echo-sounder displacement measurements, σ and ω_n were assumed equal to 1 and 0.1, respectively. Results for surge control are reported in Figs. 6 and 7, together with the required surge thrust, which has been saturated in the norm bound of 100 N.

5.2.2. P-type vs. PI-type hovering task function

Once the linear velocity controllers were tuned in order to obtain a characteristic equation with two com-plex poles in $s = -1 \pm j\,0.1$, a set of P- and PI-type guidance task functions were evaluated. The propor-tional and the integral gains for horizontal and vertical
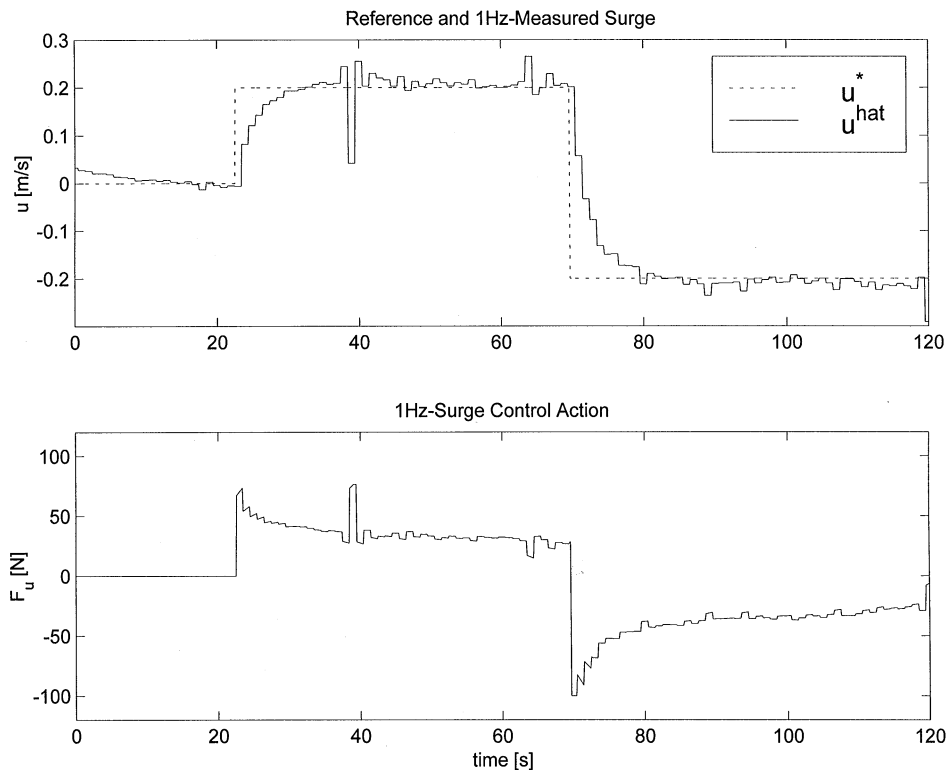

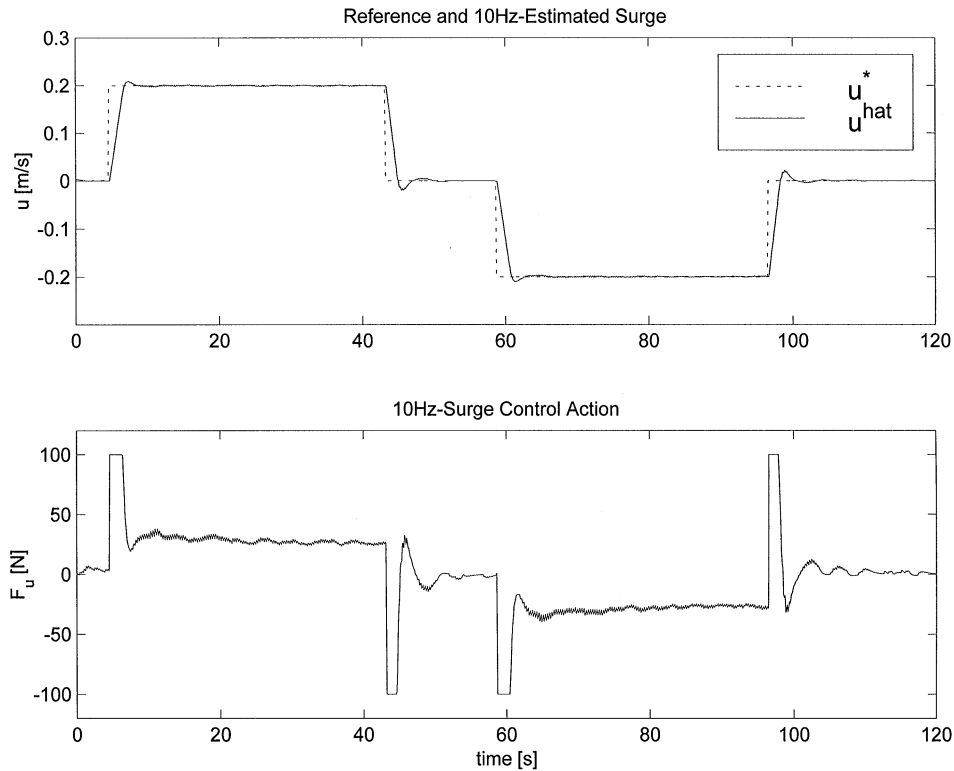Fig. 6. Surge control based on 1 Hz Doppler velocimeter speed measurement.

Fig. 7. Surge control based on 3.33 Hz echo sounder displacement measurements and eKf motion estimation.

linear position task functions were set to 0.5 and 0.1, respectively. Then the performances of P- and PI-type task functions in canceling steady-state errors due to biased speed estimates have been evaluated by means of hovering pool trials, while simulated bottom-following experiments showed the capability of the PI-type task functions in zeroing steady-state errors in the case of unmodelled kinematics interactions with the operating environment.

Hovering control. The capability of the PI-type guidance law of Eqs. (6) and (7) in zeroing steady-state errors is pointed out by the results of the hovering test reported in Figs. 8 and 9. In this experiment the vehicle was required to hover over the point (− 10, 10) m with a fixed orientation. At first, a P-type guidance algorithm was activated resulting in a steady-state error of about 3 cm along the x-axis, and 2 cm along the y-axis, respectively. After about 80 s, the operator switched on the integral action, which zeroed any position error immediately. It is worth noting that the estimates of the surge and sway were affected by a bias of about 0.5 cm/s, whose effects have been canceled by the action of the position error integrator.

Bottom-following. The capability of a PI-type guidance law in counteracting the disturbances induced by unmodelled kinematics interactions between the vehicle and the operating environment is shown by the following simulations, where the vehicle was required to maintain an altitude of 1 m moving at a surge of 0.2 m/s upwards and downwards along a bottom profile presenting a slope of about 22°. As discussed in Section 3.1.3 a simplified kinematics model $\dot{h} = -w$, neglecting the unmodelled velocity $\delta\dot{h} = -u_a \tan\alpha$, $\alpha \in (-\pi/2, \pi/2)$, due to the interactions between the vehicle's surge and the seabed slope, can be used to synthesize a bottom-following controller. In the case when a P-type guidance law is applied, a steady-state tracking error $\delta e = \delta\dot{h}/\lambda$, of about 0.16 m in this situation, occurs when the vehicle flies over the sloping bottom profile. This behaviour is shown in the upper picture of Fig. 10, where the reference and measured altitude are plotted. The vehicle ascends the profile between 30 and 70 s and descends the slope between 120 and 160 s. Since the P-type guidance gain only partially compensates for the unmodelled kinematics, steady-state conditions with remarkable tracking errors are attained. When a PI-type guidance law is applied, the integral action compensates for the unmodelled kinematics as shown in the lower picture of Fig. 10. In this case, the vehicle ascends the profile between 30 and 70 s and descends the slope between 140 and 180 s. Transient tracking errors are recorded only where discontinuities in the bottom slope occur, i.e. in the virtual velocity disturbance caused by the unmodelled kinematics.
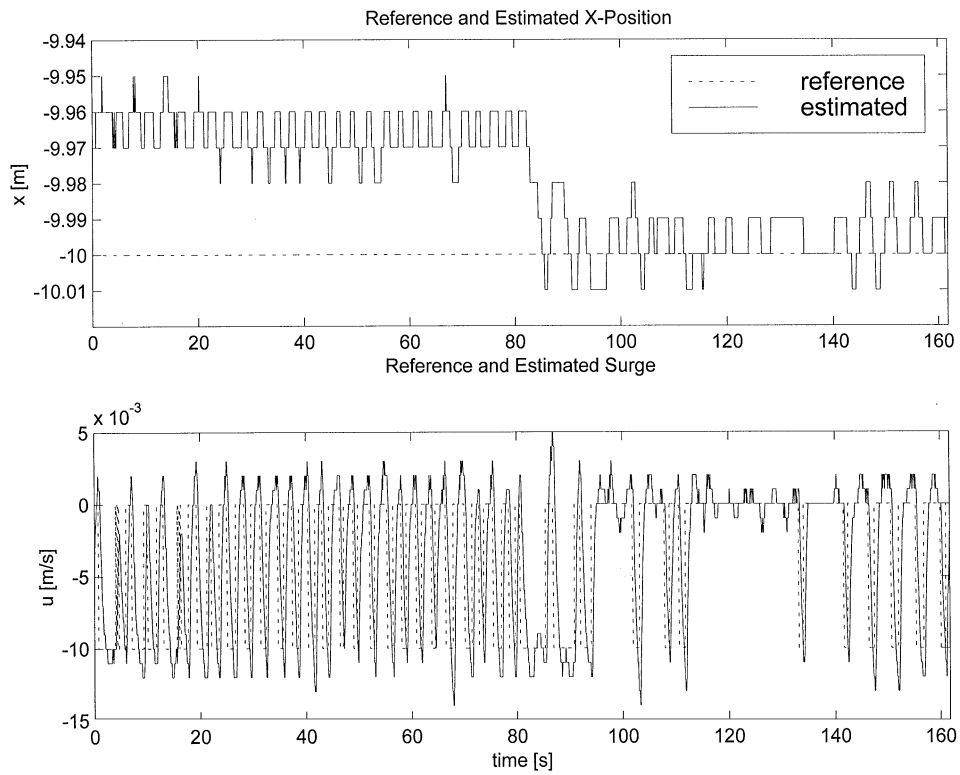
Fig. 8. P- vs. PI-type guidance: reference and estimated *x*-position and surge (the integral action is switched on after about 80 s).
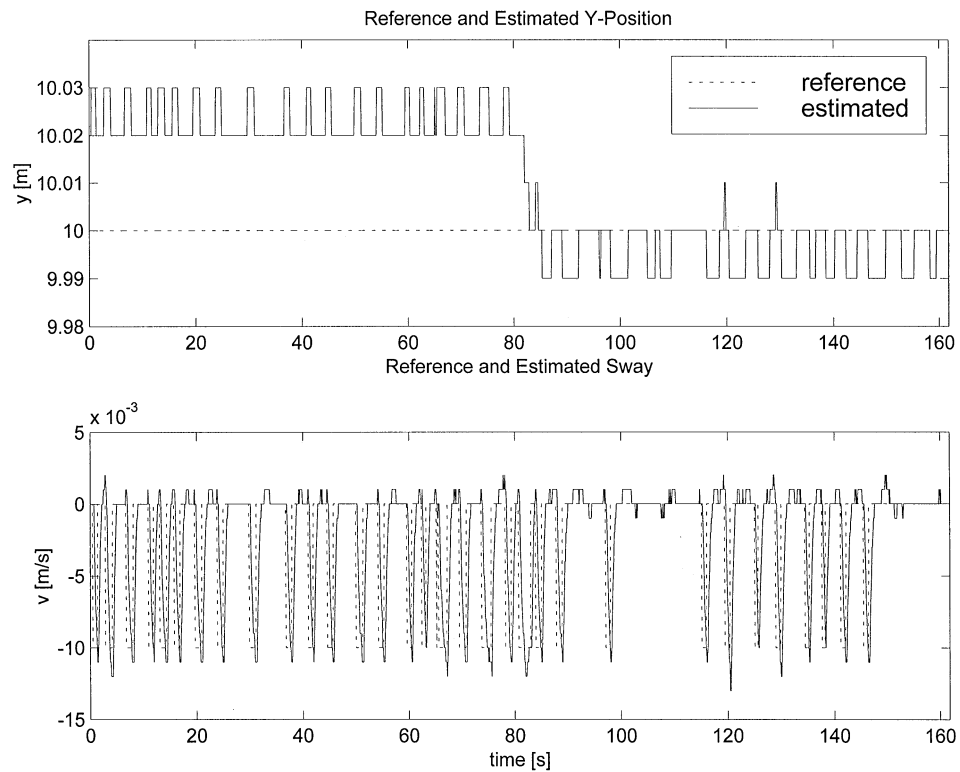

Fig. 9. P- vs. PI-type guidance: reference and estimated *y*-position and sway (the integral action is switched on after about 80 s).
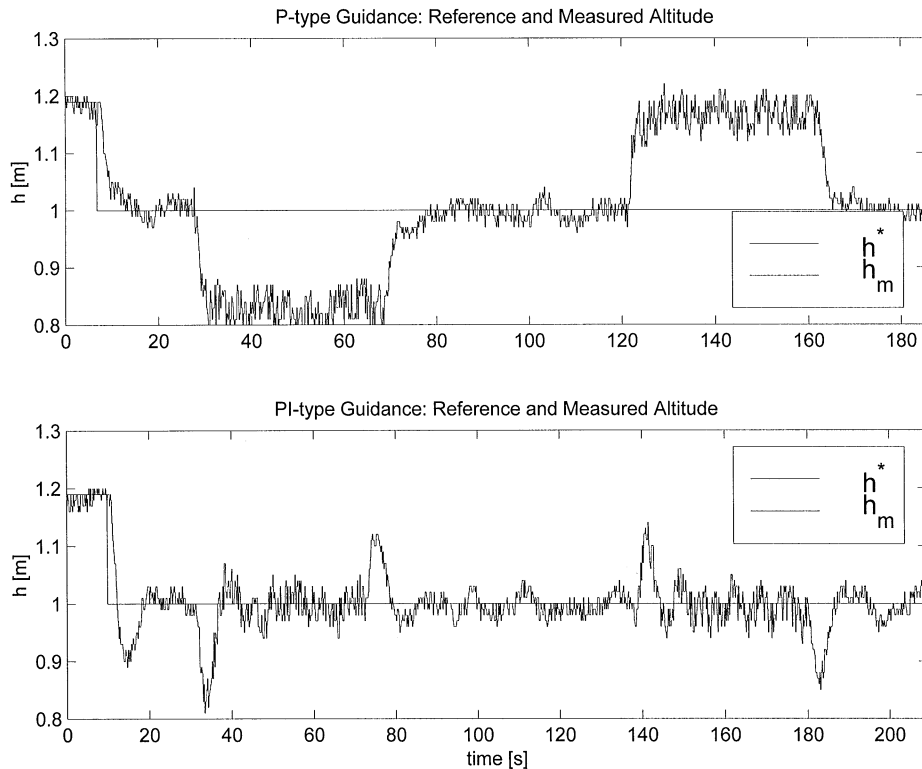
P-type Guidance: Reference and Measured Altitude

PI-type Guidance: Reference and Measured Altitude

Fig. 10. P- vs. PI-type guidance: reference and measured altitude.

5.2.3. Hovering and altitude control

The same PI-type guidance law used for Romeo hovering in the experiment of Section 5.2.2, where $\varepsilon_{ON} = 0.08$ m, $\varepsilon_{OFF} = 0.12$ m and maximum horizontal speed equal to 0.3 m/s, was applied to move Romeo towards a target, maintaining a fixed orientation. Experimental results for when the vehicle was asked to reach the point $(-10, 6)$ m are presented. The reference, measured and estimated vehicle x and y positions are plotted in Fig. 11, where the capability of the model-based Kalman filter to predict the vehicle position in presence of missed echoes and measurements outliers is shown. In particular, the continuous tracking of the pool walls and the adoption of a vehicle model that included propeller–hull interactions enhance the eKf performances with respect to the results presented in Marco and Healey (1998), where the problem of positioning the NPS Phoenix in the proximity of sonar-detected features is addressed using sliding-mode control and Kalman filtering techniques. The generated reference values for Romeo's surge and sway speeds are plotted, together with the corresponding estimates, in Fig. 12, while Fig. 13 shows the applied surge and sway control forces. It is worth noting, that thanks to the model-based feed-forward control component and smooth surge and sway estimates, the required control action is quite smooth, without any chattering. This fact is confirmed by the analysis of the applied thruster voltages, which are proportional to the desired propeller revolution rates and plotted in Fig. 14. During the experiment the thruster voltages were computed also considering the torque control action required by the autoheading task function and the corresponding yaw rate controller.

Once the vehicle was hovering over the desired point, it was possible to switch on the combined depth and altitude estimator described in Section 3.3.1, and the *auto-altitude* task function. In the case reported in Fig. 15, after about 30 s, Romeo was required to reach an altitude of 10 cm. A P-type guidance law was activated and, in order to avoid any overshoot phenomenon, the maximum heave was very low, i.e. 5 cm/s. Anyway, this constraint is fully compatible with high precision requirements for scientific low speed operations in the proximity of the seabed. As a consequence of the P-type algorithm a steady-state altitude error of about 2 cm was recorded.

5.2.4. Horizontal and vertical thrust mapping reconfigurability

So far tests have been performed on a perfectly working system with a redundant thruster configuration. In this section the behaviour of the vehicle with a different thruster configuration, as in the case when faulty thrusters have been disabled, is examined. A number of
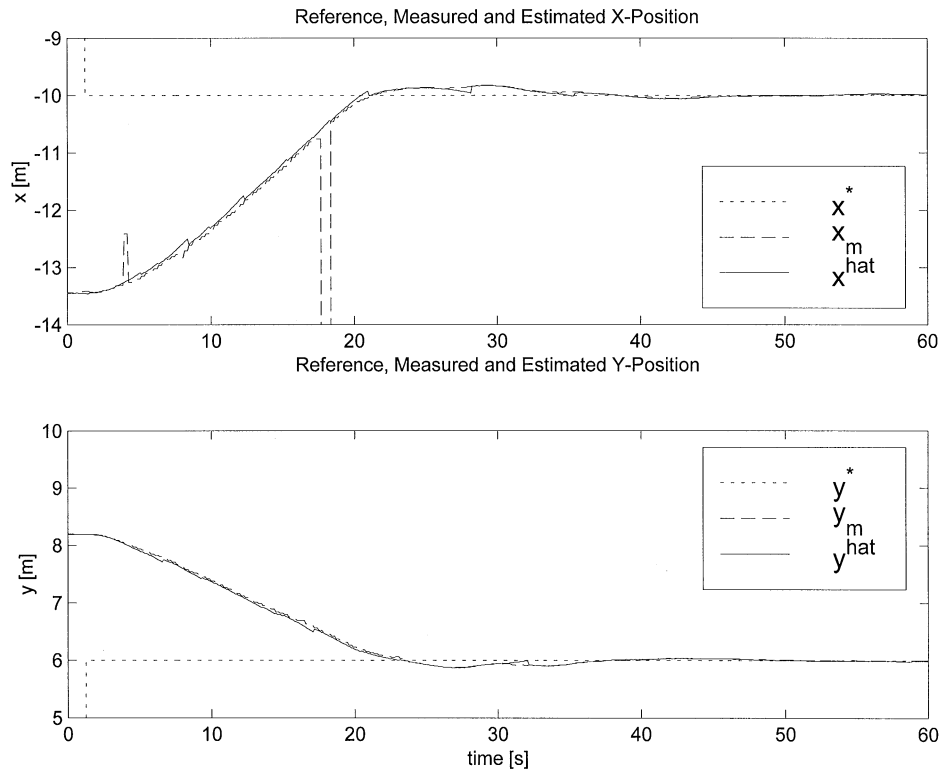
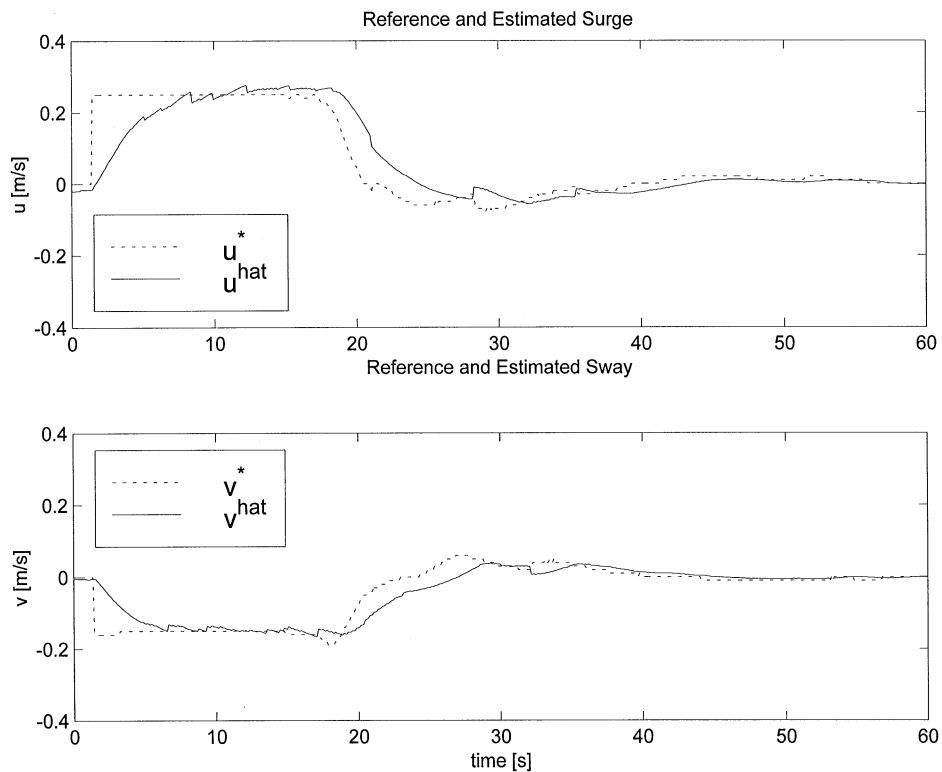Fig. 11. PI-type guidance: "go to (x, y)" task execution: reference, measured and estimated position.

Fig. 12. PI-type guidance: "go to (x, y)" task execution: reference and estimated velocities.
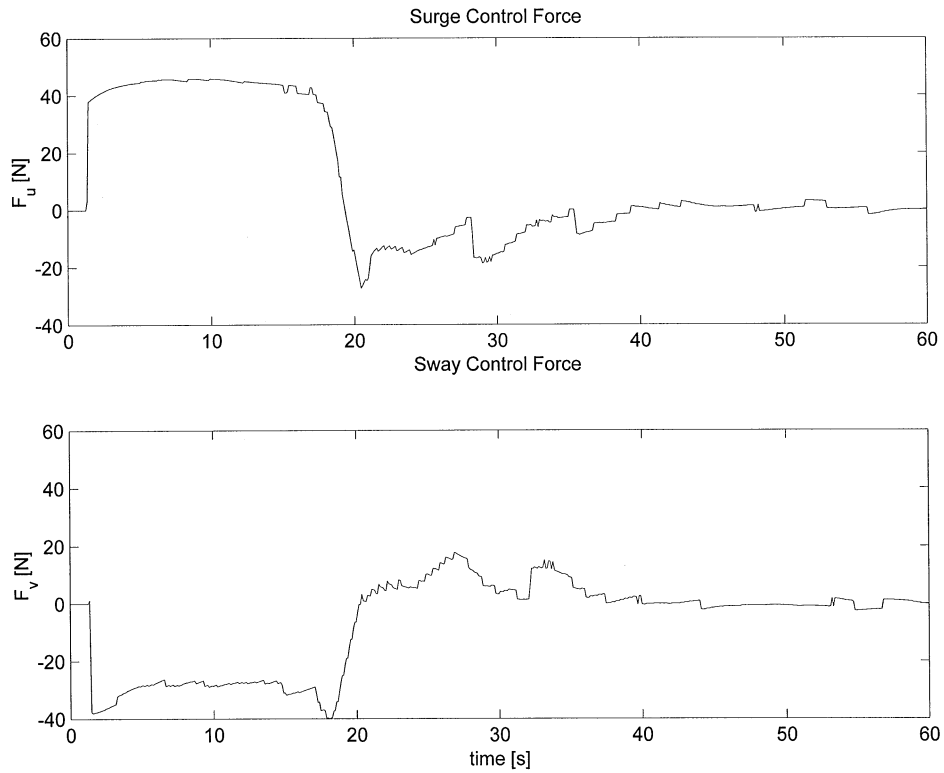
Fig. 13. PI-type guidance: "go to (x, y)" task execution: surge and sway control forces.
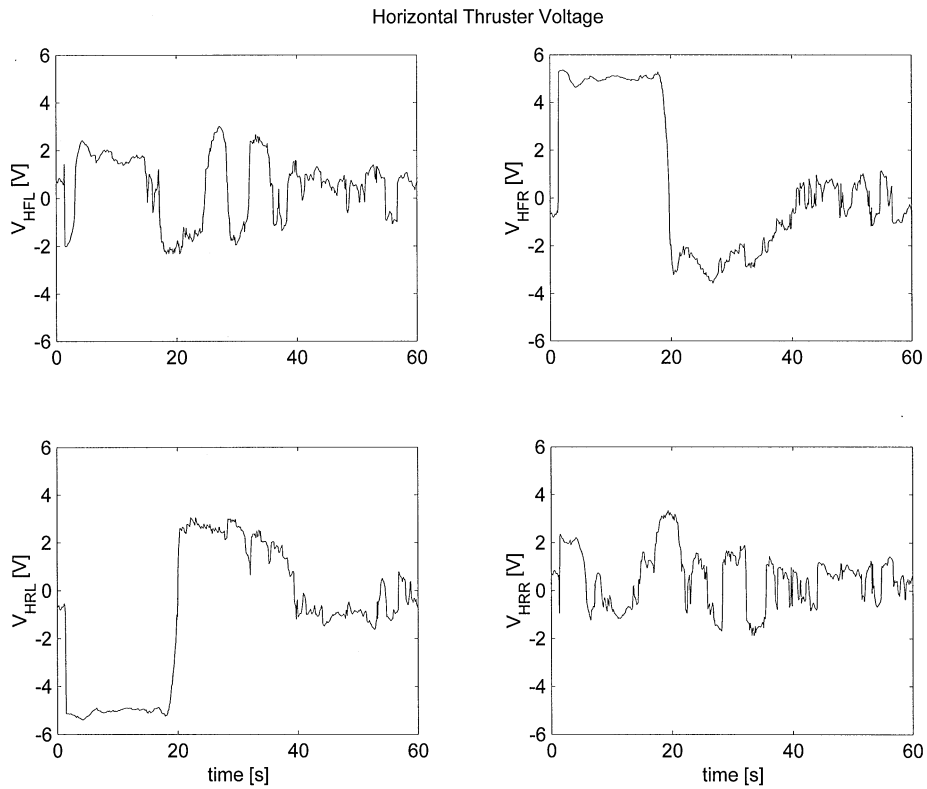

Fig. 14. PI-type guidance: "go to (x, y)" task execution: horizontal thruster voltages.
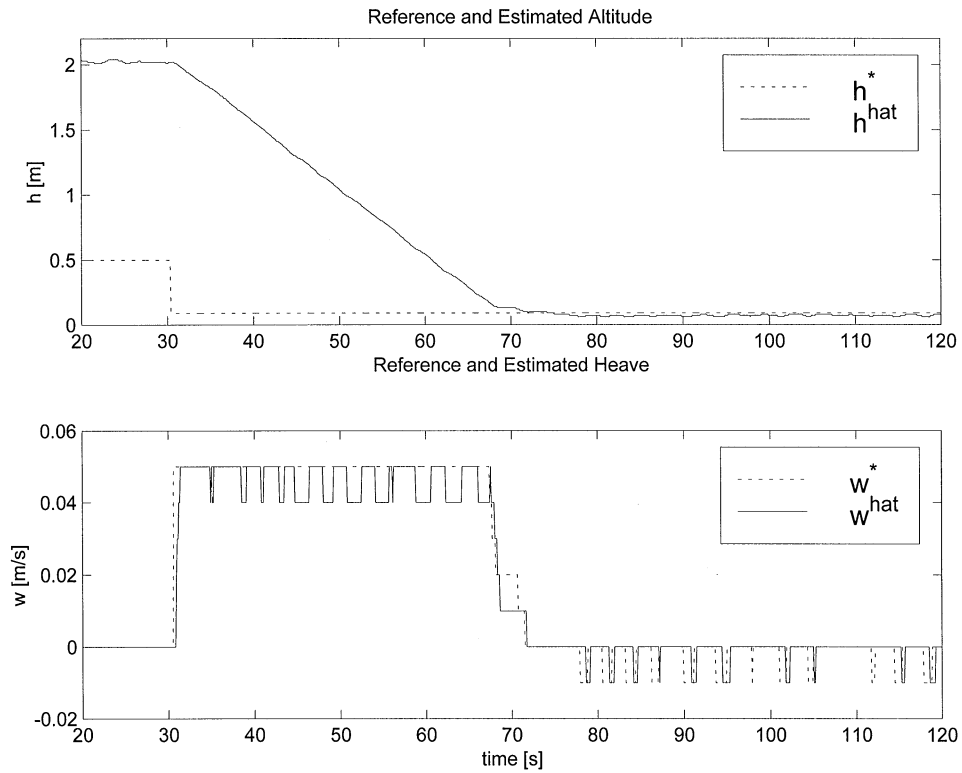
Reference and Estimated Altitude

Reference and Estimated Heave

Fig. 15. P-type guidance: "auto-altitude" task execution.

Reference and Estimated X

Reference and Estimated Y
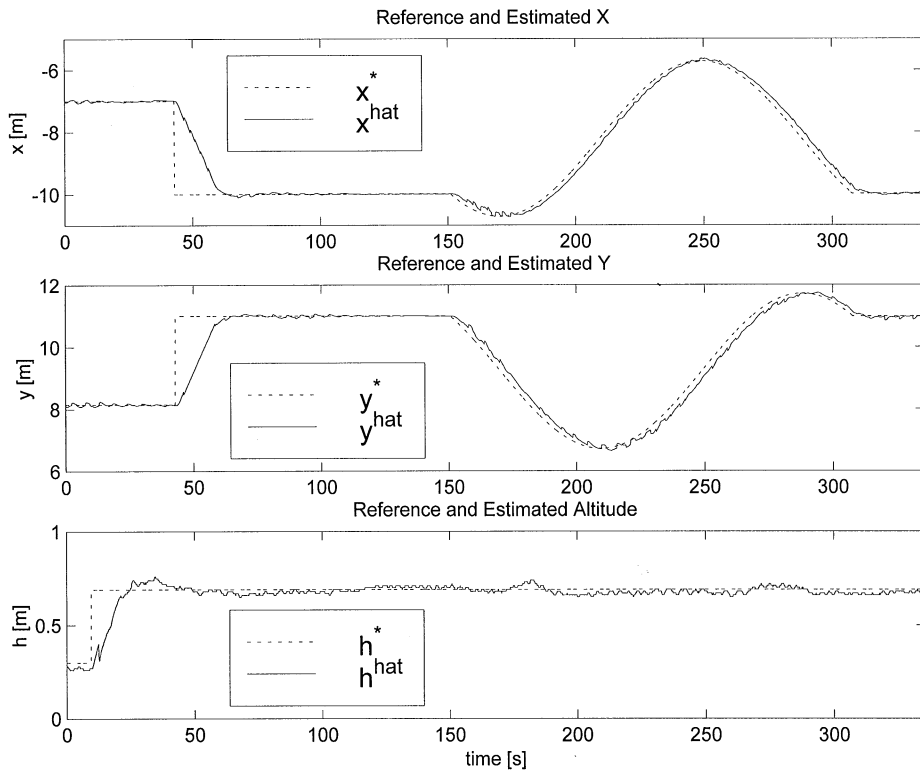
Reference and Estimated Altitude

Fig. 16. Position and altitude control without rear right thrusters.

trials simulating the need of inhibiting each thruster separately have been performed without observing any decay in the guidance and control system performances. Then the combined presence of vertical and horizontal thruster faults was simulated. As discussed in Section 5.1, since the desired vehicle pitch and roll were zero, only two diagonally opposite vertical thrusters were needed to control the vehicle depth/altitude, and three horizontal actuators to perform auto-heading and auto-speed. On the basis of these considerations, a situation in which the vertical front left and rear right thrusters and the horizontal rear right thruster were disabled has been considered. In these operational conditions, the horizontal and vertical control force–torque to actuator thrusts mapping have been computed, inverting the corresponding control matrixes.

During the experiment reported in Fig. 16, Romeo was required to change its altitude, move to the position $(-10, 11)$ m, hover over this site for more than 100 s, execute a circle and then hover $(-10, 11)$ m again, maintaining a fixed orientation parallel to the pool walls. Performances in terms of precision are comparable to those obtained with all the eight thrusters working.

6. Conclusions

Experimental tests have proved the functionality of the proposed layered hierarchical guidance and control architecture for UUVs executing high-precision near-bottom motion tasks with reconfigurable thruster configurations. In particular, remarkable performance enhancements were attained by using PI-type guidance algorithms, which were also applied to the control of the vehicle's vertical motion, by the combined estimation of the vehicle's depth and altitude in hovering conditions, and by the introduction of a lumped parameter model of the vehicle's thrusters including propeller–hull interactions. After promising results obtained in pool trials, the system is going to be tested at sea in order to check its reliability in performing on bottom scientific missions.

Acknowledgements

References

Ageev, M. D., Kasatkin, B. A., & Scherbatyuk, A. (1995). Positioning of an autonomous underwater vehicle. *Proceedings of the international program development in undersea robotics & intelligent control* (pp. 15–17). Portugal: Lisboa.

Aicardi, M., Caiti, A., Cannata, G., & Casalino, G. (1995). Stability and robustness analysis of a two layered hierarchical architecture for the closed loop control of robots in the operational space. *Proceedings of 1995 IEEE international conference on robotics and automation*, vol. 3, (pp. 2771–2778). Japan: Nagoya.

Alessandri, A., Bono R., Caccia, M., Indiveri, G., & Veruggio, G. (1998). Experiences on the modeling and identification of the heave motion of an open-frame UUV. *Proceedings of Oceans'98* (pp. 1049–1053). France: Nice.

Åström, K. J., & Wittenmark, B. W. (1989). *Adaptive Control*. USA: Addison-Wesley.

Bellingham, J. G., Goudey, C. A., Consi, T. R, Bales, J. W., Atwood, D. K., Leonard, J. J., & Chryssostomidis, C. (1994). A second generation survey AUV. *IEEE 1994 symposium on autonomous underwater vehicle technology* (pp. 148–156). USA: Cambridge.

Bennett, A. A., Leonard, J. J., & Bellingham, J. G. (1995). Bottom following for survey-class autonomous underwater vehicles. *Proceedings of the ninth international symposium on unmanned untethered submersible technology* (pp. 327–336). USA: Durham.

Caccia, M., Casalino, G., Cristi, R., & Veruggio, G. (1998). Acoustic motion estimation and control for an unmanned underwater vehicle in a structured environment. *Control Engineering Practice*, 6(5), 661–670.

Caccia, M., Bruzzone, G., & Veruggio, G. (1999a). Active sonar-based bottom following for unmanned underwater vehicles. *Control Engineering Practice*, 7(4), 459–468.

Caccia, M., Bono, R., Bruzzone, G., & Veruggio, G. (1999b). Variable configuration UUVs for marine science applications. *IEEE Robotics and Automation Magazine*, 6(2), 22–32.

Everett, H. R. (1995). *Sensors for mobile robots – Theory and application*. USA: A.K. Peters Ltd., Wellesley.

Fossen, T. I., & Sagatun, S. I. (1991). Adaptive control of nonlinear underwater robotic systems. *Proceedings of the IEEE conference on robotics and automation* (pp. 1687–1695). USA: Sacramento.

Fossen, T. I. (1994). *Guidance and control of ocean vehicles*, England: Wiley.

Fossen, T. I., & Fjellstad, I. E. (1995). Robust adaptive control of underwater vehicles: A comparative study. *Proceedings of the third IFAC workshop on control applications in marine systems* (pp. 66–74). Norway: Trondheim.

Fryxell, D., Oliveira, P., Pascoal, A., Silvestre, C., & Kaminer, I. (1996). Navigation, guidance and control of AUVs: an application to the MARIUS vehicle. *Control Engineering Practice*, 4(3), 401–409.

Healey, A. J., & Lienard, D. (1993). Multivariable sliding-mode control for autonomous diving and steering of unmanned underwater vehicles. *IEEE Journal of Oceanic Engineering*, 18(3), 327–339.

Khalil, H. K. (1996). Nonlinear systems (2nd ed.), Upper Saddle River, USA: Prentice-Hall.

Kirkwood, W. J. (1998). Tiburon: Science and technical results from MBARIs new ROV integrated to a SWATH platform. *Proceedings of Oceans'98* (pp. 1578–1583). France: Nice.

Krieg, M.L., & Gray, A.G. (1996). Performance of state space multi-sensor track fusion with model mismatch. *Proceedings of the first Australian data fusion symposium* (pp. 1–6). Australia: Adelaide.

Maddalena, D., Prendin, W., & Zampato, M. (1994). Innovations on underwater stereoscopy: The new developments of the TV-Trackmeter. *Proceedings of Oceans'94 OSATES*, vol. 2 (pp. 150–156). France: Brest.

Marco, D. B., & Healey, A. J. (1998). Local area navigation using sonar feature extraction and model-based predictive control. *International Journal of Systems Science*, 29(10), 1123–1133.

Negahdaripour, S., Xu, X., & Khamene, A. (1998). Applications of direct 3D motion estimation for underwater machine vision systems. *Proceedings of oceans'98* (pp. 51–55). France: Nice

Newman, J. B., & Stokes, D. (1994). Tiburon: Development of an ROV for ocean science research. *Proceedings of Oceans'94*, vol. 2 (pp. 483–488). France: Brest.

Newman, J. N. (1977). *Marine hydrodynamics*. Cambridge, USA: MIT Press.

Nokin, M. (1996). ROV 6000 — a deep teleoperated system for scientific use. *Proceeding of sixth IARP workshop on underwater robotics*. France: Toulon.

Nokin, M. (1998). Sea trials of the deep scientific system Victor 6000. *Proceedings of Oceans'98* (pp. 1573–1577). France: Nice.

Oliveira, P., & Pascoal, A. (1998). Navigation systems design: an application of multi-rate filtering theory. *Proceedings of Oceans'98* (pp. 1348–1353). France: Nice.

Perry Tritech Ltd. (1996). *Remotely operated vehicles of the world 1996/97 edition*. Ledbury, England: Oilfield Publications Limited.

Samson, C., Le Borgne, M., & Espiau, B. (1991). *Robot control: the task function approach*. Oxford Science Publications, Oxford Engineering Science Series, vol. 22. Oxford, Great Britain: Clarendon Press.

Sayers, C., Yoerger, D. R., & Paul, R. P. (1996). A manipulator work package for teleoperation from unmanned untethered vehicles – current feasibility and future applications. *Proceedings of the sixth international advanced robotic program*. France: Toulon.

Sheridan, T. B. (1989). Telerobotics. *Automatica, 25*(4), 487–507.

Silvestre, C., Aguiar, A., Oliveira, P., & Pascoal, A. (1998). Control of the SIRENE underwater shuttle: System design and tests at sea. *Proceedings of the 17th international conference on offshore mechanics and arctic engineering*. Portugal: Lisbon.

Singh, H., Yoerger D. R., Bachmayer R., Bradley A. M., & Stewart, W. K. (1995). Sonar mapping with the autonomous benthic explorer (ABE). *Ninth international symposium on unmanned untethered submersible technology* (pp. 367–375). USA: Durham.

Smith, C., Terribile A., & Finottello R. (1998). ARAMIS — Scientific user requirements. Contract No. MAS3-CT97-0083, *SPE-T1-001*.

Smith, S. M., Heeb, K., Frolund, N., & Pantelakis, T. (1995). The ocean explorer AUV: A modular platform for coastal oceanography. *Ninth international symposium on unmanned submersible technology* (pp. 67–76). USA: Durham.

Veruggio, G., Bono, R., Bruzzone, G., Caccia, M., & Virgili, P. (1998). A man–machine interface for the development of an innovative underwater gripper. *International Journal of System Science, 29*(5), 529–537. London: Taylor and Francis.

Yoerger, D. R., & Slotine, J. J. E. (1985). Robust trajectory control of underwater vehicles. *IEEE Journal of Oceanic Engineering,, OE-10*(4), 462–470.

Yoerger, D. R., Bradley, A. M., & Walden, B. (1993). Dynamic testing of the autonomous benthic explorer. *Eighth international symposium on unmanned untethered submersible technology* (pp. 179–188). USA: Durham.

Yuh, J. (1990). Modeling and control of underwater robotic vehicles. *IEEE Transactions on Systems, Man, and Cybernetics, 20*(6), 1475–1483.

Yuh, J. (1994). Learning control for underwater robotic vehicles. *IEEE Control Systems, 14*(2), 39–46.